A Distributed Two-Layer Framework for Teleoperated Platooning of Fixed-Wing UAVs via Decomposition and Backstepping

Minhyeong Lee and Dongjun Lee

***Abstract*—We propose a novel distributed control framework for teleoperated platooning of multiple three-dimensional (3D) fixed-wing unmanned aerial vehicles (UAVs), consisting of the following two layers: 1) *virtual frame layer*, which generates the target 3D nonholonomic motion of the virtual nonholonomic frames (VNFs) using the nonholonomic decomposition (D. J. Lee, 2010) and backstepping in such a way that the VNFs are to maintain the platoon formation in a distributed manner while respecting the directionality of the fixed-wing UAV; and 2) *local control layer*, which drives each fixed-wing UAV to track their respective VNF with their under-actuation and aerodynamic disturbance effects fully taken into account by using the backstepping and Lyapunov-based design techniques. Convergence and stability of salient aspects of each layer and their combination are theoretically established. Simulations with 25 fixed-wing UAVs and a haptic device are also performed to validate the theory with their multimedia provided at https://youtu.be/Z3Mo66KIsns.**

***Index Terms*—Decomposition, distributed robots, fixed-wing unmanned aerial vehicles (UAVs), formation control, nonholonomic constraint, platoon, teleoperation.**

I. Introduction

FORMATION control of multiple unmanned vehicles is drawing an increasing interest due to its promise to materialize numerous powerful commercial and military applications, with their implementation becoming ever closer to reality with the recent rapid advancement of hardware and software technologies. Formation control of unmanned aerial vehicles (UAVs) can further extend these applications into the three-dimensional (3D) air environment. Teleoperated platooning (i.e., the forefront leader UAV operated by a remote (or onboard) operator (e.g., via first-person view (FPV) camera), while the follower UAVs flying with certain relative spatial relation maintained among them all through the leader) is very a promising direction for this formation control, at least for the near future [2], as it allows us to incorporate human intelligence to cope with unexpected situations (often not fully resolved by the state-of-the-art autonomy) in a familiar setting (e.g., car driving), while minimizing the human-associated costs (e.g., fatigue, casualty, labor, etc.). In this letter, we consider this problem of teleoperated platooning of the fixed-wing UAVs.

The two major categories of the UAVs are the rotor-based UAVs (e.g., quadrotor drones [3]) and the fixed-wing UAVs [4]. As compared to the rotor-based UAVs, the fixed-wing UAVs are known to possess longer flying time/distance and better robustness to wind disturbance. They are however also known to be subject to the directionality constraint, that is, in a typical flying condition, their Cartesian velocity should be predominantly along the forward direction (i.e., along the main vehicle axis) to produce enough lift force for the vehicle. To address this directionality of the fixed-wing UAVs, many prior works have adopted the two-dimensional (2D) nonholonomic unicycle model (with its permissible velocity modeling the UAV's forward velocity) and proposed distributed formation control schemes for that (e.g., [5]–[9]). Yet, these 2D results (e.g., [5]–[9]) are not directly applicable to the 3D teleoperated platooning of the fixed-wing UAVs (e.g., simply augment those 2D control with some other vertical motion control), since, with the directionality, their velocity vector is rotating together with the body, thus, their motion can only be properly captured/analyzed by incorporating their full kinematics in $\mathsf{SE}(3)$.

In this letter, we propose a novel distributed two-layer control framework for the teleoperated platooning of multiple fixed-wing UAVs evolving in $\mathsf{SE}(3)$, which can accommodate arbitrary/unpredictable (remote or onboard) operator command or that from automatic mission planner. Our framework consists of the following two layers:

1) **virtual frame layer**, which generates the target 3D nonholonomic motion of virtual nonholonomic frames (VNFs) using the nonholonomic passive decomposition [1] and backstepping in such a way that the VNFs are guaranteed to maintain the platoon formation among them in a distributed manner (i.e., requiring only peer-to-peer (P2P) communication); and
2) **local control layer**, which drives each physical fixed-wing UAV to track the target 3D nonholonomic motion of their respective VNF with the effects of their control under-actuation and the aerodynamic disturbance fully

Manuscript received October 15, 2020; accepted February 16, 2021. Date of publication March 8, 2021; date of current version March 25, 2021. This letter was recommended for publication by Associate Editor I. Manchester and Editor P. Pounds upon evaluation of the reviewers' comments. This work was supported by a Grant to Bio-Mimetic Robot Research Center funded by Defense Acquisition Program Administration, and by Agency for Defense Development of Korea (UD190018ID). *(Corresponding author: Dongjun Lee.)*

The authors are with the Department of Mechanical Engineering, IAMD and IER, Seoul National University, Seoul 08826, South Korea (e-mail: minhyeong@snu.ac.kr; djlee@snu.ac.kr).

This letter has supplementary downloadable material available at https://doi.org/10.1109/LRA.2021.3064207, provided by the authors.

Digital Object Identifier 10.1109/LRA.2021.3064207

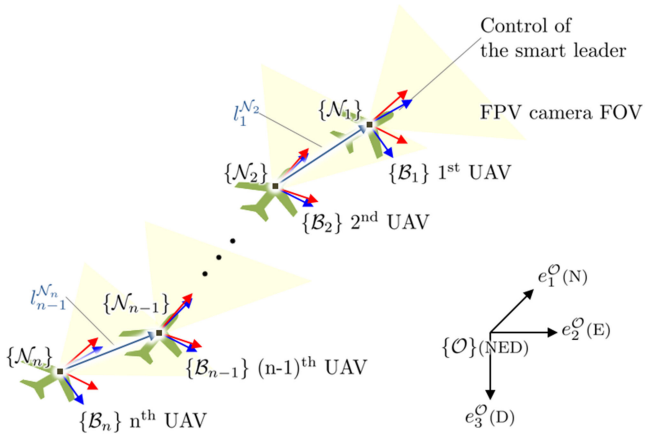

Fig. 1. Frames of the teleoperated platooning control: $l_j \in \mathbb{R}^3$, expressed in the $(j+1)$-th VNF $\{\mathcal{N}_{j+1}\}$, specifies the desired relative position between $\{\mathcal{N}_j\}$ and $\{\mathcal{N}_{j+1}\}$, and each j-th UAV's body-frame $\{\mathcal{B}_j\}$ follows the trajectory of its corresponding VNF $\{\mathcal{N}_j\}$.

taken into account by using the backstepping and the Lyapunov-based control design techniques.

See Fig. 1 for an illustration of the teleoperated platooning. Our framework renders the multiple fixed-wing UAVs to behave as a deformable string or structure "pulled by" one of its corners [10] - see Section IV. Although our framework can accommodate other formation shapes, in this letter, we also focus on the line-topology platooning as shown in Fig. 1, since it allows the multiple UAVs to navigate through obstacles or pass through a narrow passage one by one via their collective serpentine motion, particularly relevant to urban air mobility (UAM) scenarios.

In contrast to many results for the 2D nonholonomic agents (e.g., [5]-[9]), those for the distributed formation control of 3D nonholonomic agents are very rare and, to our knowledge, the recent works of [11], [12] are the only results for this. The results of [11], [12], however, are not fully distributed, as they assume each agent have access to the leader's attitude; and do not fully consider the underlying dynamics of the fixed-wing UAV either, which is not nonholonomically constrained but under-actuated. On the other hand, backstepping [13] has been widely-used for the control of a *single* under-actuated system (e.g., [3]), however, not has been so for the distributed control of multiple agents in $\mathsf{SE}(3)$. One of rare results for this is [14], where a distributed formation control was presented for the rotor-based UAVs in $\mathsf{SE}(3)$ on a balanced graph. This rotor-based UAV is however omni-directional (i.e., can assume any Cartesian velocity w.r.t. the body), thus, the nonholonomic constraint adopted in this letter to respect the directionality of the fixed-wing UAVs is not necessary therein. To our knowledge, our proposed framework is the very first result for the distributed control of the fixed-wing UAVs, which can fully incorporate their directionality and kinematics in $\mathsf{SE}(3)$ by utilizing the nonholonomic decomposition [1] and backstepping, while also ensuring the robustness against the aerodynamic disturbance and well-behaving of the attitude motion even under their under-actuation by utilizing the Lyapunov-based control design and backstepping. This adoption of backstepping renders our framework inherently robust following the well-known robustness property of the backstepping [13]. This current letter also extends our prior result of [15] for the 2D kinematic nonholonomic unicycles to the 3D under-actuated dynamic fixed-wing UAVs.

The rest of the letter is organized as follows. Section II introduce the virtual frame layer and its distributed VNF platooning strategy based on the nonholonomic decomposition and backstepping. The local control layer for each fixed-wing UAV is detailed in Section III based on the backstepping and Lyapunov-based design. Simulations of teleoperated platooning with 25 fixed-wing UAVs are performed in Section IV. Section V concludes the letter.

II. Virtual Frame Layer

A. Nonholonomic Decomposition of VNFs

Let us consider the VNF $\{\mathcal{N}_j\}$ for the j-th UAV evolving in $\mathsf{SE}(3)$, whose Cartesian position is denoted by $p_{N_j} \in \mathbb{R}^3$ and its rotation matrix by $R_{N_j} \in \mathsf{SO}(3)$. The position and the rotation are expressed w.r.t. the north-east-down (NED) inertial frame $\{\mathcal{O}\}$ with its vectors being e_1, e_2, e_3 for the N, E, and D directions. The kinematics of $\{\mathcal{N}_j\}$ is then given by:

$$\dot{p}_{N_j} = R_{N_j} v_{N_j} \quad \text{and} \quad \dot{R}_{N_j} = R_{N_j} \hat{\omega}_{N_j} \tag{1}$$

where $v_{N_j} \in \mathbb{R}^3$ is the velocity and $\omega_{N_j} \in \mathbb{R}^3$ is the angular rate with hat map $\hat{\cdot}: \mathbb{R}^3 \to \mathsf{so}(3)$, which is a skew-symmetric operator satisfying $\hat{x}y = x \times y$ for all $x, y \in \mathbb{R}^3$. The motion of the VNF $\{\mathcal{N}_j\}$ can then be described by

$$T_j := \begin{bmatrix} R_{N_j} & p_{N_j} \\ 0_{1\times 3} & 1 \end{bmatrix} \in \mathsf{SE}(3) \quad \text{and} \quad \xi_j := \begin{pmatrix} v_{N_j} \\ \omega_{N_j} \end{pmatrix} \in \mathbb{R}^6$$

where T_j is the transformation matrix in the special Euclidean group, ξ_j is the spatial velocity or so-called the (body) twist in screw theory, and $0_{a\times b} \in \mathbb{R}^{a\times b}$ is a zero matrix.

In order to capture the directionality of the fixed-wing UAV, that is, the majority of its velocity is along its forward direction while its sideways velocities are much smaller, we set the following nonholonomic constraint:

$$A\xi_j = 0_{2\times 1} \tag{2}$$

with $A := (0_{2\times 1}, I_2, 0_{2\times 3}) \in \mathbb{R}^{2\times 6}$ and $I_a \in \mathbb{R}^{a\times a}$ is a identity matrix. Note that this constraint (2) ensures the sideways velocities of the VNF are zero (i.e., $e_2^T v_{N_j} = e_3^T v_{N_j} = 0$).

To attain the platooning behavior in a distributed manner, we design the virtual frame layer action for each pair of a preceding j-th VNF and its following $(j+1)$-th VNF. For this, we define the pairwise twist as

$$\xi_{j,j+1} := \begin{pmatrix} \xi_j \\ \xi_{j+1} \end{pmatrix} \in \mathbb{R}^{12}$$

with the pairwise nonholonomic constraint:

$$\mathrm{diag}(A, A)\xi_{j,j+1} = 0_{4\times 1} \tag{3}$$

where $\mathrm{diag}(\cdots)$ is a block diagonal matrix operator. From the constraint (3), we define the *unconstrained distribution* [1] as

$$\mathcal{D}^\top := \mathrm{diag}(e_1, I_3, e_1, I_3) \in \mathbb{R}^{12\times 8} \tag{4}$$

which characterizes the null-space of $\mathrm{diag}(A, A)$ in (3). Every possible twist of the VNF should satisfy $\xi_{j,j+1} \in \mathrm{col}(\mathcal{D}^\top)$, where $\mathrm{col}(\cdot)$ is a column space operator.

The platooning behavior can then be attained by enforcing the following pairwise virtual constraint:

$$h_{j,j+1} := p_{N_j} - p_{N_{j+1}} - R_{N_{j+1}} l_j = 0_{3\times 1} \tag{5}$$

where $h_{j,j+1} \in \mathbb{R}^3$ is called a formation map [1] and $l_j \in \mathbb{R}^3$ is the relative position vector expressed in $\{\mathcal{N}_j\}$. This constraint (5) ensures that the relative position of the preceding VNF as observed in the following VNF is equal to l_j, i.e., $R_{N_{j+1}}^T(p_{N_j} - p_{N_{j+1}}) = l_j$, with the trailing condition $l_j^{(1)} := e_1^T l_j > 0$ also assumed. This also means that the preceding VNF is within the limited field-of-view of the following VNF, pointing the direction of l_j, regardless of the formation shape and its curvature [15]. Note also that $h_{j,j+1}$ can be understood as a formation error in the inertial frame. See Fig. 1 for an illustration of the platooning under (5). We now state the control objective of the virtual frame layer to achieve the platooning among the VNFs by enforcing (5).

Control objective 1: Consider the VNFs $\{\mathcal{N}_j\}$ evolving in $\mathsf{SE}(3)$ under the nonholonomic constraint (2). We then want to enforce $h_{j,j+1} \to 0_{3\times 1}$ with its twist $\xi_j \in \mathbb{R}^6$ also bounded for all VNFs.

From the constraint (5), we define the *normal distribution*:

$$\Delta_{j,j+1}^{\perp} := \begin{bmatrix} R_{N_j} & 0_3 & -R_{N_{j+1}} & R_{N_{j+1}}\hat{l}_j \end{bmatrix}^T \in \mathbb{R}^{12\times 3}$$

with $\frac{\mathrm{d}}{\mathrm{d}t} h_{j,j+1} = (\Delta_{j,j+1}^{\perp})^T \xi_{j,j+1}$. The orthogonal complement of this normal distribution is named as *tangential distribution* and obtained by

$$\Delta_{j,j+1}^{\top} := \begin{bmatrix} I_3 & 0_3 & -R_{N_{j,j+1}}\hat{l}_j \\ 0_3 & I_3 & 0_3 \\ R_{N_{j,j+1}}^T & 0_3 & 0_3 \\ 0_3 & 0_3 & I_3 \end{bmatrix} \in \mathbb{R}^{12\times 9}$$

where $R_{N_{j,j+1}} := R_{N_j}^T R_{N_{j+1}}$ is the relative rotational matrix. This $\Delta_{j,j+1}^{\top}$ characterizes the twist tangential to the level set:

$$\mathcal{H}_{h_{j,j+1}} := \{(T_a, T_b) \mid T_a, T_b \in \mathsf{SE}(3), h(T_a, T_b) = h_{j,j+1}\}$$

i.e., $\frac{\mathrm{d}}{\mathrm{d}t} h_{j,j+1} = 0_{3\times 1}$, while the normal distribution indicates the twist normal to the level set $\mathcal{H}_{h_{j,j+1}}$.

We decompose the unconstrained distribution (4) under the virtual constraint (5) by the *locked and quotient distributions* [1] as follows. The locked distribution is the intersection between the unconstrained and tangential distributions s.t. $\mathcal{D}_{j,j+1}^{l} := \mathcal{D}^{\top} \cap \Delta_{j,j+1}^{\top}$, which stands for the twist space enforcing $h_{j,j+1}$ fixed while satisfying the nonholonomic constraint (3). There exists a subspace of $\mathrm{col}(\mathcal{D}_{j,j+1}^{l})$ which does not affect the preceding twist ξ_j. It does not appear in the 2D results of [15] as it determines the roll rate of the VNF. For this, we define a new distribution $\mathcal{D}_{j+1} := [0_6; I_6] \in \mathbb{R}^{12\times 6}$ which characterize only the follower's motion. Then, we can decompose the locked distribution according to the dependency on ξ_j into 1) the j-independent locked distribution:

$$\mathcal{D}_{j,j+1}^{li} := \mathcal{D}_{j,j+1}^{l} \cap \mathcal{D}_{j+1} = \frac{1}{l_j^{(1)}} \begin{bmatrix} 0_{3\times 1} \\ 0_{3\times 1} \\ 0_{3\times 1} \\ l_j \end{bmatrix} \in \mathbb{R}^{12\times 1} \quad (6)$$

and 2) the j-dependent locked distribution:

$$\mathcal{D}_{j,j+1}^{ld} := \mathcal{D}_{j,j+1}^{l} \setminus \mathcal{D}_{j,j+1}^{li} = \frac{1}{l_j^{(1)}} \begin{bmatrix} l_j^{(1)} e_1 & 0_3 \\ 0_{3\times 1} & l_j^{(1)} I_3 \\ e_1 l_j^T R_{N_{j,j+1}}^T e_1 & 0_3 \\ \hat{e}_1 R_{N_{j,j+1}}^T e_1 & 0_3 \end{bmatrix} \in \mathbb{R}^{12\times 4} \quad (7)$$

where $\mathrm{col}(\mathcal{D}_{j,j+1}^{l}) = \mathrm{col}([\mathcal{D}_{j,j+1}^{li}, \mathcal{D}_{j,j+1}^{ld}])$.

One the other hand, the quotient distribution is a relative complement of the locked distribution w.r.t. the unconstrained distribution s.t.

$$\mathcal{D}_{j,j+1}^{c} := \mathcal{D}^{\top} \setminus \mathcal{D}_{j,j+1}^{l} = \frac{1}{l_j^{(1)}} \begin{bmatrix} -l_j^{(1)} D_{(1,0,0)} \\ 0_3 \\ e_1 l_j^T R_{N_{j,j+1}}^T \\ \hat{e}_1 R_{N_{j,j+1}}^T \end{bmatrix} \in \mathbb{R}^{12\times 3} \quad (8)$$

where $D_{(a,b,c)} = \mathrm{diag}(a, b, c) \in \mathbb{R}^{3\times 3}$ is a diagonal matrix. The quotient distribution contains both the normal and tangential components to the level set $\mathcal{H}_{h_{j,j+1}}$ [15]. Complete normal-tangential decoupling is possible only if the strong decomposability is granted [1], which is not the case here.

From the decomposition, the pairwise twist can be written by

$$\xi_{j,j+1} = \underbrace{\begin{bmatrix} \mathcal{D}_{j,j+1}^{li} & \mathcal{D}_{j,j+1}^{ld} & \mathcal{D}_{j,j+1}^{c} \end{bmatrix}}_{=:S_{j,j+1}\in\mathbb{R}^{12\times 8}} \begin{pmatrix} u_{LI_{j,j+1}} \\ u_{LD_{j,j+1}} \\ u_{C_{j,j+1}} \end{pmatrix} \quad (9)$$

where $S_{j,j+1}$ is the decomposition matrix [15] and $u_{\star_{j,j+1}}$ are the inputs for the virtual frame layer, which are to be distributed in Section II-B. From now on, let us omit the subscript $\{j, j+1\}$ to shorten notations, for instance, $h := h_{j,j+1}$, $R_N := R_{N_{j,j+1}}$, $\Delta^{\star} := \Delta_{j,j+1}^{\star}$, $\mathcal{D}^{\star} := \mathcal{D}_{j,j+1}^{\star}$, and $u_{\star} := u_{\star_{j,j+1}}$. Then, the distribution inputs to be designed are $u_{LI} \in \mathbb{R}$, $u_{LD} \in \mathbb{R}^4$, and $u_C \in \mathbb{R}^3$.

B. Distributed Virtual Layer Input Design

As in (9), the distribution inputs $u_{\star}$ directly specify the twist. If we directly assign the inputs, however, the VNF acceleration may not be smooth, which is incompatible with the local tracking control in Section III, as it requires the jerk of position. Thus, in this Section II-B, we design update laws of $\dot{\omega}_{N_{j+1}}, \dot{v}_{N_{j+1}}$ for the VNFs to maintain the platooning while being compatible with the local control in Section III.

Let us define the reference inputs $u_{LI}^{\mathrm{ref}} \in \mathbb{R}$, $u_{LD}^{\mathrm{ref}} \in \mathbb{R}^4$, and $u_C^{\mathrm{ref}} \in \mathbb{R}^3$ instead of directly defining their real inputs $u_{\star}$. Writing the first six rows of (9) with the reference distribution inputs, we get

$$\xi_j^{\mathrm{ref}} = \begin{bmatrix} e_1 & 0_3 \\ 0_{3\times 1} & I_3 \end{bmatrix} u_{LD}^{\mathrm{ref}} + \begin{bmatrix} -D_{(1,0,0)} \\ 0_3 \end{bmatrix} u_C^{\mathrm{ref}} \in \mathbb{R}^6$$

from (6), (7), and (8). Suppose that the preceding twist ξ_j and its derivatives are already given. Choosing the condition of the reference inputs as $\xi_j^{\mathrm{ref}} = \xi_j$, the following equality $u_{LD}^{\mathrm{ref}} = (e_1^T(v_{N_j} + u_C^{\mathrm{ref}}); \omega_{N_j})$ must be satisfied. Substituting this equality to (9) and extracting the last six rows, we can

compute the reference twist of the following frame by

$$\xi^{\mathrm{ref}}_{j+1} = \frac{1}{l^{(1)}_j}\begin{bmatrix} e_1 l_j^T \\ \hat{e}_1 \end{bmatrix} R_N^T (v_{N_j} + D_{(2,1,1)} u^{\mathrm{ref}}_C) + \frac{1}{l^{(1)}_j}\begin{bmatrix} 0_{3\times 1} \\ l_j \end{bmatrix} u^{\mathrm{ref}}_{LI} \in \mathbb{R}^6 \tag{10}$$

with $\xi^{\mathrm{ref}}_{j+1} := (v^{\mathrm{ref}}_{N_{j+1}}; \omega^{\mathrm{ref}}_{N_{j+1}})$, where $v^{\mathrm{ref}}_{N_{j+1}}, \omega^{\mathrm{ref}}_{N_{j+1}} \in \mathbb{R}^3$ are the reference velocity and angular rate. Note that u^{ref}_{LI} rotates $\{\mathcal{N}_{j+1}\}$ along its l_j direction and the rotation is tangential to the level set $\mathcal{H}_{h_{j,j+1}}$, while u^{ref}_C can change the formation (5). Once the reference distribution inputs are determined, the update laws of $\dot{\omega}_{N_{j+1}}, \ddot{v}_{N_{j+1}}$ can be specified by backstepping approach as below, for which u^{ref}_{LI} needs to be differentiable and u^{ref}_C twice differentiable.

1) Roll Motion of VNF: The attitude of $\{\mathcal{N}_{j+1}\}$, especially its roll motion, is introduced to determine u^{ref}_{LI}, since the distribution input determines the roll rate by $e_1^T \omega^{\mathrm{ref}}_{N_{j+1}} = u^{\mathrm{ref}}_{LI}$. Here, we develop an update law of u^{ref}_{LI} to mimic the under-actuated roll motion for better compatibility with the physics of the fixed-wing UAVs.

One of the common roll motion of the fixed-wing UAVs is to use a desired bank angle (i.e., roll angle of fixed-wing aircraft) as in [16], where the desired bank angle can be obtained by its steering acceleration and the gravitational acceleration $g > 0$. Thus, we define the sum of the accelerations as

$$a_{j+1.g} := \bar{\omega}^{\mathrm{ref}}_{N_{j+1}} \times v^{\mathrm{ref}}_{N_{j+1}} - g R^T_{N_{j+1}} e_3 \in \mathbb{R}^3$$

where $\bar{\omega}^{\mathrm{ref}}_{N_{j+1}} := \omega^{\mathrm{ref}}_{N_{j+1}} - (l_j/l^{(1)}_j) u^{\mathrm{ref}}_{LI} \in \mathbb{R}^3$ is independent of the roll rate (or u^{ref}_{LI}) from (10). Then our bank angle error is

$$\varphi_{j+1} := \arctan2(a^{(2)}_{j+1.g}, -a^{(3)}_{j+1.g}) \in \mathbb{R}$$

where $a^{(2)}_{j+1.g} = e_2^T a_{j+1.g} \in \mathbb{R}$ and $a^{(3)}_{j+1.g} = e_3^T a_{j+1.g} \in \mathbb{R}$. Using the error, we design the update law of the roll rate:

$$\dot{u}^{\mathrm{ref}}_{LI} = -b_\omega u^{\mathrm{ref}}_{LI} - k_\omega(-\vartheta_{j+1}) \tag{11}$$

$$\dot{\vartheta}_{j+1} + u^{\mathrm{ref}}_{LI} = -b_\vartheta \vartheta_{j+1} + k_\vartheta \varphi_{j+1} \tanh(\|D_{(0,1,1)} a_{j+1.g}\|_2 / g) \tag{12}$$

where $b_\omega, b_\vartheta > 0$ are stabilizing gains, $k_\omega, k_\vartheta > 0$ are driving gains, $\vartheta_{j+1} \in \mathbb{R}$ is the "filtered" bank angle error approaching to the bank angle error φ_{j+1}. The new variable ϑ_{j+1} is introduced here to avoid a direct impact of φ_{j+1} on u^{ref}_{LI}. In (12), we use $\dot{\vartheta}_{j+1} + u^{\mathrm{ref}}_{LI}$, since ϑ_{j+1} evolves on the VNF, whose roll rate is u^{ref}_{LI}. The hyperbolic tangent function discounts the effect of the bank angle error when $a^{(2)}_{j+1.g}, a^{(3)}_{j+1.g}$ are both small. Considering the matrix form of (11), (12), we can find exponentially stable control gains $b_\omega, k_\omega, b_\vartheta$. In the steady state, we also have

$$u^{\mathrm{ref}}_{LI} = \frac{k_\vartheta}{1 + b_\vartheta b_\omega / k_\omega} \varphi_{j+1} \tanh(\|D_{(0,1,1)} a_{j+1.g}\|_2 / g)$$

and it is the same as the conventional bank angle control, which determines the roll rate with the bank angle error. Geometric relations of this roll rate control are visualized in Fig. 2.

2) Virtual Constraint and Backstepping: Let us consider the virtual constraint (5) to determine the reference quotient distribution input u^{ref}_C with the first Lyapunov function:

$$V_1 := \frac{1}{2} h^T h \tag{13}$$

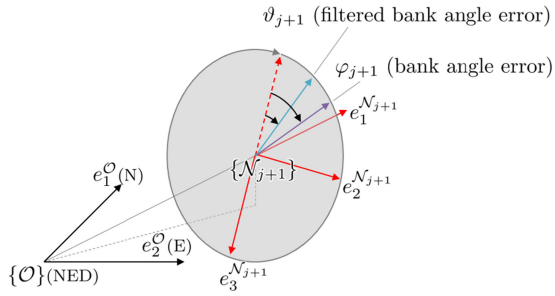

Fig. 2. The filtered bank angle error ϑ_{j+1} approaches to the bank angle error φ_{j+1} from (12), and the roll motion of the VNF follows ϑ_{j+1} from (11).

which is positive definite. The time derivative of (13) yields

$$\begin{aligned}\dot{V}_1 &= h^T \frac{\mathrm{d}h}{\mathrm{d}t} = h^T (\Delta^\perp)^T \begin{pmatrix} \xi_j \\ \xi_{j+1} \end{pmatrix} \\ &= h^T (\Delta^\perp)^T \begin{pmatrix} \xi_j \\ \xi^{\mathrm{ref}}_{j+1} \end{pmatrix} + h^T (\Delta^\perp)^T \begin{pmatrix} 0_{6\times 1} \\ e_{\xi_{j+1}} \end{pmatrix} \\ &= h^T (\Delta^\perp)^T \mathcal{D}^c u^{\mathrm{ref}}_C + \nu_1^T B \Delta^\perp h\end{aligned}$$

with the fact that $(\Delta^\perp)^T \mathcal{D}^{li} = 0_{3\times 1}$ and $(\Delta^\perp)^T \mathcal{D}^{lr} = 0_{3\times 4}$. The twist error is denoted by $e_{\xi_{j+1}} := \xi_{j+1} - \xi^{\mathrm{ref}}_{j+1}$ and it can be squeezed into $\nu_1 := B(0_{6\times 1}; e_{\xi_{j+1}}) \in \mathbb{R}^4$ with

$$B := \begin{bmatrix} 0_{1\times 6} & e_1^T & 0_{1\times 3} \\ 0_{3\times 6} & 0_3 & I_3 \end{bmatrix} \in \mathbb{R}^{4\times 12}$$

while it can be reconstructed by $(0_{6\times 1}; e_{\xi_{j+1}}) = B^T \nu_1$. To establish the stability, we set the reference quotient distribution input by

$$u^{\mathrm{ref}}_C = -K_h (\mathcal{D}^c)^T \Delta^\perp h = K_h D_{(2,1,1)} R_{N_j} h \tag{14}$$

We then have $\dot{V}_1 = -k_h h^T h + \nu_1^T B \Delta^\perp h$, where $k_h > 0$ is a positive constant and $K_h := k_h D^{-1}_{(4,1,1)}$ is a positive definite matrix. Note that (14) is a twice differentiable equation.

We get u^{ref}_{LI} from (11), (12) and u^{ref}_C from (14). Substituting these reference distribution inputs to (10), we can compute the reference twist ξ^{ref}_{j+1} and its derivatives. Now the backstepping approach is employed to obtain the update laws of the twist. For this, we augment a quadratic potential of ν_1 to (13) by

$$\begin{aligned} V_2 &:= \frac{1}{2} h^T h + \frac{1}{2\gamma_1} \nu_1^T \nu_1 \\ \dot{V}_2 &= -k_h h^T h + \frac{1}{\gamma_1} \nu_1^T (\dot{\nu}_1 + \gamma_1 B \Delta^\perp h) \end{aligned} \tag{15}$$

with a constant $\gamma_1 > 0$, which leads us to an update law:

$$\dot{\nu}_1 = -k_1 \nu_1 - \gamma_1 B \Delta^\perp h + C^T \nu_2$$

with $k_1 > 0$ and $C := (1, 0_{1\times 3}) \in \mathbb{R}^{1\times 4}$, where $\nu_2 := C(\dot{\nu}_1 + k_1 \nu_1 + \gamma_1 B \Delta^\perp h) \in \mathbb{R}$ is the remained error of the update law on the velocity aspect. From the update law, the derivative of the angular rate is designated as

$$\dot{\omega}_{N_{j+1}} = \dot{\omega}^{\mathrm{ref}}_{N_{j+1}} - k_1 e_{\omega_{N_{j+1}}} + \gamma_1 \hat{l}_j R^T_{N_{j+1}} h \tag{16}$$

where $e_{\omega_{N_{j+1}}} := \omega_{N_{j+1}} - \omega^{\mathrm{ref}}_{N_{j+1}}$ is the angular rate error. Similarly, we augment a quadratic potential of ν_2 to (15)

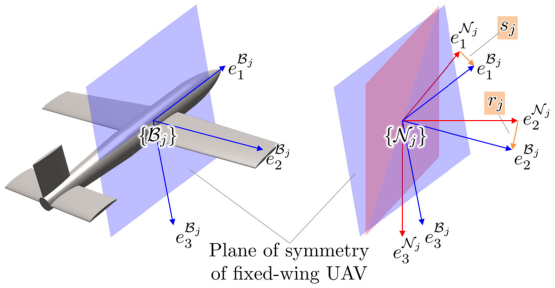

Fig. 3. Heading-hold control aims to regulate the symmetric plane alignment error r_j and the heading vector error s_j as much as permissible by the higher priorities in the null-space hierarchical control (27).

by

$$V_3 := \frac{1}{2}h^T h + \frac{1}{2\gamma_1}\nu_1^T\nu_1 + \frac{1}{2\gamma_1\gamma_2}\nu_2^T\nu_2$$
$$\dot{V}_3 = -k_h h^T h - \frac{k_1}{\gamma_1}\nu_1^T\nu_1 + \frac{1}{\gamma_1\gamma_2}\nu_2^T(\dot{\nu}_2 + \gamma_2 C\nu_1) \tag{17}$$

with a constant $\gamma_2 > 0$. Then it suggests an update law:

$$\dot{\nu}_2 = -k_2\nu_2 - \gamma_2\, C\nu_1$$

so that we can obtain $\dot{V}_3 = -k_h h^T h - \frac{k_1}{\gamma_1}\nu_1^T\nu_1 - \frac{k_2}{\gamma_1\gamma_2}\nu_2^T\nu_2$ which is negative definite with a constant $k_2 > 0$. The update law then derives

$$\ddot{v}_{N_{j+1}} = \ddot{v}^{\mathrm{ref}}_{N_{j+1}} - (k_1+k_2)\dot{e}_{v_{N_{j+1}}} - (k_1k_2+\gamma_2)e_{v_{N_{j+1}}}$$
$$- \gamma_1 D_{(1,0,0)}\left(\frac{\mathrm{d}}{\mathrm{d}t}(R^T_{N_{j+1}}h) + k_2 R^T_{N_{j+1}}h\right) \tag{18}$$

where $e_{v_{N_{j+1}}} := v_{N_{j+1}} - v^{\mathrm{ref}}_{N_{j+1}}$ is the velocity error. The following Prop. 1 summarizes the main properties of our virtual frame layer control and the attainment of the Control objective 1 in Section II-A. Note also that, from the twist updates of the virtual frame layer (16) and (18), we can calculate the acceleration of $(j+1)$-th VNF by $\ddot{p}_{N_{j+1}} = R_{N_{j+1}}(\dot{v}_{N_{j+1}} + \hat{\omega}_{N_{j+1}}v_{N_{j+1}})$ and the jerk by $\dddot{p}_{N_{j+1}} = R_{N_{j+1}}(\ddot{v}_{N_{j+1}} + 2\hat{\omega}_{N_{j+1}}\dot{v}_{N_{j+1}} + \dot{\hat{\omega}}_{N_{j+1}}v_{N_{j+1}} + \hat{\omega}^2_{N_{j+1}}v_{N_{j+1}})$, which are to be used for the local control layer in Section III.

Proposition 1: Consider the VNFs (1) and their reference twists given by (10) with (11), (12) and (14). Then, the reference velocity is twice differentiable and the reference angular rate is differentiable. Further, with the update laws, (16) and (18), the formation objective (5) is achieved (i.e., $h_{j,j+1} \to 0_{3\times1}$) exponentially and the twist of each VNF also converges to their respective reference twist (i.e., $\xi_{j+1} \to \xi^{\mathrm{ref}}_{j+1}$) exponentially.

Proof: See the Lyapunov function (17) and its time derivative $\dot{V}_3 \le -2\min(k_h, k_1, k_2)V_3$. Then, V_3 exponentially converges to zero and so do h, ν_1, and ν_2. The last item follows from $\xi_{j+1} = \xi^{\mathrm{ref}}_{j+1} + [0_{6\times6}, I_6]B^T\nu_1$. ■

III. Local Control Layer

This Section III-A presents the local control layer, which aims to drive each fixed-wing UAV to track their respective VNF $\{\mathcal{N}_j\}$ robustly even with their under-actuation. For this, let us attach a frame $\{\mathcal{B}_j\}$ to the j-th UAV, whose e_1, e_2, e_3 represent the heading, main-wing, and down direction as in Fig. 3. We then model the fixed-wing UAV as a combination of the translation dynamics and the attitude kinematics of $\{\mathcal{B}_j\}$ evolving in $\mathsf{SE}(3)$ with the assumption of availability of low-level attitude control:

$$m_j\ddot{p}_{B_j} = R_{B_j}f_j + m_j g e_3 \tag{19}$$
$$\dot{R}_{B_j} = R_{B_j}\hat{\omega}_{B_j} \tag{20}$$

where $m_j \in \mathbb{R}$ is the mass, $p_{B_j} \in \mathbb{R}^3$ is the position vector, $R_{B_j} \in \mathsf{SO}(3)$ is the rotation matrix, $\omega_{B_j} \in \mathbb{R}^3$ is the body angular rate, and $f_j \in \mathbb{R}^3$ is a force on the body-fixed frame written by

$$f_j := f^t_j e_1 + f^v_j(\rho, v_j)$$

where $f^t_j \in \mathbb{R}$ is the thrust control input, $f^v_j(\rho, v_j) \in \mathbb{R}^3$ is the aerodynamic force of the fixed-wing UAV as modeled in [17], $\rho \in \mathbb{R}$ is the temperature/altitude-dependent air density, $v_j := R^T_{B_j}(\dot{p}_{B_j} - v_w) \in \mathbb{R}^3$ is the relative wind velocity, and $v_w \in \mathbb{R}^3$ is the wind velocity in $\{\mathcal{O}\}$ measurable as stated in [18]. In this letter, we consider uncertainty only in the aerodynamic force $f^v_j(\rho, v_j)$, as this is typically much larger as compared to other uncertainties (e.g., inertia parameters, control/communication imperfectness, etc.).

Control objective 2: Consider the fixed-wing UAV (19), (20) evolving in $\mathsf{SE}(3)$. We then want the position p_{B_j} of the UAV to track that of its VNF (i.e., p_{N_j}), and its attitude R_{B_j} matches that of the VNF (i.e., R_{N_j}) as much as permissible (i.e., within the null-space of the (p_{B_j}, p_{N_j})-tracking objective - see (27)), while ensuring robustness against the aerodynamic uncertainty and boundedness of all the states even with their under-actuation.

A. Position Tracking Control Design

We first consider the position tracking problem between the fixed-wing UAV and its corresponding VNF. For this, we extend the framework of [3] to the case of fixed-wing UAVs. Define a desired acceleration for the position tracking:

$$a^{\mathrm{des}}_j := \ddot{p}_{N_j} - b_a\dot{e}_j - k_a e_j = \ddot{p}_{B_j} + \nu_a \in \mathbb{R}^3$$

where $e_j := p_{B_j} - p_{N_j} \in \mathbb{R}^3$ is the position error between the UAV and its VNF, and $\nu_a \in \mathbb{R}^3$ is the acceleration error due to the under-actuation. To enforce $e_j, \dot{e}_j \to 0_{3\times1}$, we define $\zeta_j := (\dot{e}_j; e_j) \in \mathbb{R}^6$ and the following Lyapunov function:

$$W_1 := \frac{1}{2}\zeta_j^T P\zeta_j$$
$$\dot{W}_1 = -\zeta_j^T Q\zeta_j - \nu_a^T(\dot{e}_j + \epsilon e_j) \tag{21}$$

with 6×6 matrices:

$$P := \begin{bmatrix} 1 & \epsilon \\ \epsilon & k_a + \epsilon b_a \end{bmatrix} \otimes I_3,\ Q := \begin{bmatrix} b_a - \epsilon & 0 \\ 0 & \epsilon k_a \end{bmatrix} \otimes I_3 \in \mathbb{R}^{6\times6}$$

where $\otimes$ is the Kronecker product. This P, Q are both positive definite if we choose a small ϵ s.t. $0 < \epsilon < b_a$. For backstepping, we augment W_1 and obtain:

$$W_2 := \frac{1}{2}\zeta_j^T P\zeta_j + \frac{1}{2\gamma}\nu_a^T\nu_a$$
$$\dot{W}_2 = -\zeta_j^T Q\zeta_j + \frac{1}{\gamma}\nu_a^T(\dot{\nu}_a - \gamma(\dot{e}_j + \epsilon e_j)) \tag{22}$$

where $\gamma > 0$ is a constant. This then suggests us the following update law:

$$\dot{\nu}_a = u_{\nu_a} := -k\nu_a + \gamma(\dot{e}_j + \epsilon e_j) \in \mathbb{R}^3 \tag{23}$$

so that $\dot{W}_2 = -\zeta_j^T Q \zeta_j - \frac{k}{\gamma}\nu_a^T \nu_a$ become negative definite, where $k > 0$ is a constant backstepping gain.

To attain the control law, we differentiate (19) by

$$m_j(\dot{a}_j^{\text{des}} - \dot{\nu}_a) = m_j \ddot{\overline{p}}_{B_j} = R_{B_j}\hat{\omega}_{B_j} f_j + R_{B_j}(\dot{f}_j^t e_1 + \dot{f}_j^v)$$

with $\dot{f}_j^v = \frac{\partial f_j^v}{\partial v_j}\dot{v}_j + \frac{\partial f_j^v}{\partial \rho}\dot{\rho}$ and $\dot{v}_j = -\hat{\omega}_{B_j} v_j + R_{B_j}^T(\ddot{p}_{B_j} - \dot{v}_w)$. The air density ρ is typically slowly varying, thus, we assume $\dot{\rho} \approx 0$. We rearrange the above equation by $G_1 u_{B_j} = d_1$ with

$$\begin{aligned} G_1 &:= \begin{bmatrix} e_1 & \frac{f_j^v}{v_j}\hat{v}_j - \hat{f}_j \end{bmatrix} \in \mathbb{R}^{3\times 4} \\ d_1 &:= -\frac{f_j^v}{v_j} R_{B_j}^T(\ddot{p}_{B_j} - \dot{v}_w) \\ &\quad + m_j R_{B_j}^T(\dot{a}_j^{des} - u_{\nu_a}) \in \mathbb{R}^3 \end{aligned} \tag{24}$$

for the UAV control input $u_{B_j} := (\dot{f}_j^t; \omega_{B_j}) \in \mathbb{R}^4$. Here, notice the redundancy from (24), that is, the size of the control input $\mathbb{R}^4$ is larger than that of the position tracking objective $\mathbb{R}^3$. Thus, we can introduce another control objective, heading-hold objective as detailed in the next Section III-B, using the null-space hierarchical control.

B. Heading-Hold Control Design

Recall from Section II that the VNF does not have sideways velocities and follows the conventional roll attitude control. This means that conditions for heading-hold can be achieved by matching the plane of symmetry of the fixed-wing UAV (a plane perpendicular to its main-wing) with that of the VNF. Thus the objective function can be written by $\dot{r}_j = -k_r r_j$, where $r_j := (R_{B_j} - R_{N_j})e_2$ is the symmetric plane error as shown in Fig. 3 and $k_r > 0$ is a positive gain. This objective function can then be organized into $G_2 u_{B_j} = d_2$ with

$$\begin{aligned} G_2 &:= \begin{bmatrix} 0_{3\times 1} & -\hat{e}_2 \end{bmatrix} \in \mathbb{R}^{3\times 4} \\ d_2 &:= R_{B_j}^T R_{N_j} \hat{\omega}_{N_j} e_2 - k_r(I_3 - R_{B_j}^T R_{N_j}) e_2 \in \mathbb{R}^3 \end{aligned} \tag{25}$$

Since G_2 in (25), together with G_1 in (24), is still lacking in spanning $\mathbb{R}^4$ (i.e., $\text{rank}([G_1; G_2]) < 4$ for some rare cases), we additionally define the third objective function as $\dot{s}_j = -k_s s_j$ where $s_j := (R_{B_j} - R_{N_j})e_1$ is the heading vector error as shown in Fig. 3 and $k_s > 0$ is a positive gain. Then, similarly to (25), we can obtain $G_3 u_{B_j} = d_3$ with

$$\begin{aligned} G_3 &:= \begin{bmatrix} 0_{3\times 1} & -\hat{e}_1 \end{bmatrix} \in \mathbb{R}^{3\times 4} \\ d_3 &:= R_{B_j}^T R_{N_j} \hat{\omega}_{N_j} e_1 - k_r(I_3 - R_{B_j}^T R_{N_j}) e_1 \in \mathbb{R}^3 \end{aligned} \tag{26}$$

This last objective (26) turns out to be very rarely activated, since, in almost all cases, $\text{rank}([G_1; G_2]) = 4$ and the lowest priority is to be assigned to (26).

More precisely, we combine (24), (25) and (26) into a form of the null-space hierarchical control s.t.

$$\begin{aligned} u_{B_j,1} &= G_1^+ d_1 \\ u_{B_j,2} &= u_{B_j,1} + P_1(G_2 P_1)^+(d_2 - G_2 u_{B_j,1}) \\ (\dot{f}_j^t; \omega_{B_j}) &= u_{B_j,2} + P_2(G_3 P_2)^+(d_3 - G_3 u_{B_j,2}) \end{aligned} \tag{27}$$

where $(\cdot)^+$ is a Moore-Penrose pseudoinverse operator, and $P_1 := I - G_1^+ G_1$, $P_2 := P_1 - (G_2 P_1)^+ G_2 P_1$ are the projection matrices into their respective null-spaces.

Proposition 2: Consider the fixed-wing UAV (19), (20) and its corresponding VNF $\{\mathcal{N}_j\}$ under the null-space hierarchical control (27) with the objectives (24), (25) and (26). Assume that: a) $(\dot{p}_{N_j}, \ddot{p}_{N_j}, \ddot{\overline{p}}_{N_j}, \omega_{N_j})$ of the VNF $\{\mathcal{N}_j\}$ are bounded; and b) the wind velocity $v_w(t)$ and the aerodynamic force $f_j^v(\rho, v_j)$ are Lipschitz continuous and bounded. Then, 1) if $f_j^v(\rho, v_j)$ is certain, the tracking error converges to zero (i.e., $\zeta_j \to 0_{6\times 1}$ and $\nu_a \to 0_{3\times 1}$) exponentially; 2) if $f_j^v(\rho, v_j)$ has a Lipschitz continuous and bounded additive uncertainty, with its magnitude and that of its derivative not so large (i.e., $|\lambda_{\max}(H)| < 1$ - see after (28)), there exist control gains for which (ζ_j, ν_a) is ultimately bounded; and 3) for both cases, UAV control input $(\dot{f}_j^t, \omega_{B_j})$ is bounded.

Proof: The null-space hierarchical control (27) satisfies the first control objective (24) if f_j^v is certain. Then we have $\dot{W}_2 \leq -2\min(\lambda_{\min}(Q)/\lambda_{\max}(P), k) W_2$ where $\lambda_{\min}(\cdot), \lambda_{\max}(\cdot)$ are the minimum and maximum eigenvalue operators. This implies $W_2 \to 0$ exponentially and so do (ζ_j, ν_a).

In order to deal with the aerodynamic uncertainty, the aerodynamic force is set to $f_j^v = \bar{f}_j^v + \tilde{f}_j^v$ where $\bar{f}_j^v(\rho, v_j) \in \mathbb{R}^3$ is the modeled aerodynamic force and $\tilde{f}_j^v(\rho, v_j) \in \mathbb{R}^3$ is the additive uncertainty. If the body acceleration $\ddot{p}_{B_j}$ can be measured with some sensors (e.g., accelerometer), we can obtain ν_a, $\dot{a}_j^{\text{des}}$, and f_j^v but cannot compute their derivatives so that the controller implements $\partial \bar{f}_j^v / \partial v_j$ instead of $\partial f_j^v / \partial v_j$ in (24). In the case that the body acceleration $\ddot{p}_{B_j}$ cannot be measured due to some practical reasons, whose proof is provided in this Prop. 2, the controller also estimates the acceleration by $\ddot{p}_{B_j} - R_{B_j}\tilde{f}_j^v / m_j$ and estimates $\dot{a}_j^{\text{des}}, u_{\nu_a}$ using the estimated acceleration. Then the tracking objective implementation (24) is replaced by $\bar{G}_1 u_{B_j} = \bar{d}_1$ with

$$\begin{aligned} \bar{G}_1 &:= \begin{bmatrix} e_1 & \frac{\bar{f}_j^v}{v_j}\hat{v}_j - \hat{\bar{f}}_j^v - f_j^t \hat{e}_1 \end{bmatrix} \in \mathbb{R}^{3\times 4} \\ \bar{d}_1 &:= -\frac{\bar{f}_j^v}{v_j} R_{B_j}^T(\ddot{p}_{B_j} - R_{B_j}\tilde{f}_j^v / m_j - \dot{v}_w) \\ &\quad + m_j R_{B_j}^T(\dot{a}_j^{\text{des}} - u_{\nu_a}) + (b_a + k)\tilde{f}_j^v \in \mathbb{R}^3 \end{aligned} \tag{28}$$

For further development, we define $H := G_1 \bar{G}_1^+ - I_3 \in \mathbb{R}^{3\times 3}$ and $F := (1/m_j)(\partial \tilde{f}_j^v / \partial v_j - H \partial \bar{f}_j^v / \partial v_j) \in \mathbb{R}^{3\times 3}$, which are both bounded (i.e., $\sigma_H : v_j \mapsto |\lambda_{\max}(H)|$ and $\sigma_F : v_j \mapsto |\lambda_{\max}(F)|$ are bounded for all v_j) due to assumptions. Then the evolution of the translation dynamics can be written by

$$\begin{aligned} \dot{\nu}_a = u_{\nu_a} &- H_O(\dot{a}_j^{\text{des}} - u_{\nu_a}) - F_O(\ddot{p}_{B_j} - \dot{v}_w) \\ &- \frac{1}{m_j} R_{B_j}(I_3 + H)\left(\frac{\partial \bar{f}_j^v}{\partial v_j}\frac{\tilde{f}_j^v}{m_j} + (b_a + k)\tilde{f}_j^v\right) \end{aligned}$$

where $H_O := R_{B_j} H R_{B_j}^T, F_O := R_{B_j} F R_{B_j}^T \in \mathbb{R}^{3\times 3}$. Note $\dot{a}_j^{\text{des}} - u_{\nu_a} = \ddot{\overline{p}}_{N_j} + (b_a + k)\nu_a + (b_a^2 - \gamma)\dot{e}_j + (b_a k_a - \gamma\epsilon)e_j$ and $\ddot{p}_{B_j} - \dot{v}_w = \ddot{p}_{N_j} - \dot{v}_w - \nu_a - b_a \dot{e}_j - k_a e_j$ while $\|H_O \ddot{\overline{p}}_{N_j} + F_O(\ddot{p}_{N_j} - \dot{v}_w) + (1/m_j) R_{B_j}(I_3 + H)((\frac{\partial \bar{f}_j^v}{\partial} v_j)$

$\tilde{f}_j^v/m_j + (b_a+k)\tilde{f}_j^v)\|_2 < \delta$ is also bounded due to assumptions. The time derivative of the Lyapunov function is now bounded by

$$\dot{W}_2 \leq -\min\left(\lambda_{\min}(Q), k/\gamma\right)\|(\zeta_j;\nu_a)\|_2^2 + (\delta/\gamma)\|\nu_a\|_2 + (\sigma_H\kappa_H/\gamma + \sigma_F\kappa_F/\gamma)\|(\zeta_j;\nu_a)\|_2^2$$

where $\kappa_H := \max(b_a+k, |b_a^2-\gamma|, |b_a k_a - \gamma\epsilon|) \in \mathbb{R}$ and $\kappa_F := \max(1, b_a, k_a) \in \mathbb{R}$ with $\|\nu_a\|_2 \leq \|(\zeta_j;\nu_a)\|_2$. The following inequality sandwiches the Lyapunov function by

$$(1/2)\min\left(\lambda_{\min}(P), 1/\gamma\right)\|(\zeta_j;\nu_a)\|_2^2 \leq W_2 \leq (1/2)\max\left(\lambda_{\max}(P), 1/\gamma\right)\|(\zeta_j;\nu_a)\|_2^2$$

so that the error (ζ_j, ν_a) converges to the bounded ball of radius $\frac{\delta/\gamma}{\min(\lambda_{\min}(Q),k/\gamma)-\sigma_H\kappa_H/\gamma-\sigma_F\kappa_F/\gamma}\sqrt{\frac{\max(\lambda_{\max}(P),1/\gamma)}{\min(\lambda_{\min}(P),1/\gamma)}}$ if $\sigma_H\kappa_H/\gamma + \sigma_F\kappa_F/\gamma < \min(\lambda_{\min}(Q), k/\gamma)$ holds. Note that we can always find a set of control gains satisfying the convergence condition if the magnitude of the uncertainty and its derivative meets $\sigma_H(v_j) < 1$.

On the other hand, with the assumed boundedness of $(\dot{p}_{N_j}, \ddot{p}_{N_j}, \dddot{p}_{N_j}, \omega_{N_j}, v_w(t), f_j^v(\rho, v_j))$ and the convergence of (ζ_j, ν_a), we can show that $\dot{p}_{B_j}, v_j, a_j^{\text{des}}, \ddot{p}_{B_j}, \dot{a}_j^{\text{des}}$ are bounded and so are d_1, d_2, d_3 as well. This then implies $(\dot{f}_j^t, \omega_{B_j})$ is bounded with $\text{rank}([G_1; G_2; G_3]) = 4$. ■

On top of Prop. 1 and Prop. 2 for the control objective achievement and the well-behaving of the relevant states in the virtual frame layer and the local control layer, respectively, we also provide the following Thm. 1 to further specify the key properties of the combined teleoperated platooning behavior of the multiple under-actuated fixed-wing UAVs.

Theorem 1: Consider the teleoperated platoon consists of n-VNFs (1) and n-fixed-wing UAVs (19), (20) with the virtual frame layer (16), (18) and the local control layer (27). Suppose that: a) the wind velocity $v_w(t)$ and aerodynamic disturbance $f_j^v(\rho, v_j)$ in (19) are Lipschitz continuous and bounded; and b) the twist ξ_1 and its derivatives $\dot{\xi}_1, \ddot{v}_{N_1}$ of the forefront (commanding) leader VNF are bounded. Then, the formation objective and the tracking objective exponentially converge, i.e., $h_{j,j+1} \to 0_{3\times 1}$ (with $\xi_{j+1} \to \xi_{j+1}^{\text{ref}}$) for $\forall j = 1, 2, \cdots n$ and $\zeta_j \to 0_{6\times 1}$ for $j = 1, 2, \cdots n$ (or ζ_j ultimately bounded with the aerodynamic uncertainty as stated in Prop. 2). Further, the control inputs of the VNFs $(\dot{\omega}_{N_{j+1}}, \ddot{v}_{N_{j+1}})$ and the UAVs $(\dot{f}_j^t, \omega_{B_j})$ are also remained to be bounded.

Proof: Note that this Thm. 1 is essentially a combination of Prop. 1 and Prop. 2 using the integrated Lyapunov function $V := \sum_{j=1}^{n-1} V_{3_{(j,j+1)}} + \sum_{j=1}^{n} W_{2_j}$ with $V_{3_{(j,j+1)}}(t), W_{2_j}(t) \to 0$ exponentially following their respective Prop. 1 and Prop. 2.

Only the exception for that is to replace the assumption a) of Prop. 2 with the boundedness assumption on $\xi_1, \dot{\xi}_1, \ddot{v}_{N_1}$ of the leader UAV. For this, assume that $\xi_j, \dot{\xi}_j, \ddot{v}_{N_j}$ are bounded for any j. Then, $u_{LI}^{\text{ref}}, \dot{u}_{LI}^{\text{ref}}$ are bounded from (11), (12). From the $h \to 0_{3\times 1}$ exponentially, we can also show that u_C^{ref} from (14) is bounded and then ξ_{j+1}^{ref} is bounded. Using the boundedness of $\nu_1 \to 0_{4\times 1}$, we get bounded ξ_{j+1} and following $\dot{h}, \dot{u}_C^{\text{ref}}, \dot{\xi}_{j+1}^{\text{ref}}$ are also bounded. Again with bounded $\nu_2 \to 0$, the twist rate $\dot{\xi}_{j+1}$ is bounded and $\ddot{h}, \ddot{u}_C^{\text{ref}}, \ddot{v}_{N_{j+1}}$ are bounded. As a result, $\xi_{j+1}, \dot{\xi}_{j+1}, \ddot{v}_{N_{j+1}}$ are all bounded if $\xi_j, \dot{\xi}_j, \ddot{v}_{N_j}$ are bounded. Thus, bounded $\xi_1, \dot{\xi}_1, \ddot{v}_{N_1}$ ensures the boundedness of the control input $(\dot{\omega}_{N_j}, \ddot{v}_{N_j})$ of all the VNFs and that of the UAV control input $(\dot{f}_j^t, \omega_{B_j})$ while nullifying the necessity of the assumption a) of Prop. 2. ■

IV. Simulation

In order to validate our proposed framework, we perform real-time simulations with a human operator in the loop. A commercial Omega.3[1] is used as a haptic device and its 3DOF Cartesian position $u_{\text{user}} \in \mathbb{R}^3$ is used to control the forefront leader VNF $\{\mathcal{N}_1\}$. For this, we set the reference acceleration for $\{\mathcal{N}_1\}$ to be $e_1^T \dot{v}_{N_1}^{\text{ref}} = \eta_1 e_1^T u_{\text{user}}$, the reference yaw rate $e_3^T \omega_{N_1}^{\text{ref}} = -\eta_2 e_2^T u_{\text{user}}$, and the reference pitch rate $e_2^T \omega_{N_1}^{\text{ref}} = -\eta_3 e_3^T u_{\text{user}}$, where $\eta_1, \eta_2, \eta_3 > 0$ are to scale the user device input. The reference roll rate $e_1^T \omega_{N_1}^{\text{ref}}$ is derived from (11), (12). The twist update law of the forefront VNF is written by

$$\dot{\omega}_{N_1} = \dot{\omega}_{N_1}^{\text{ref}} - k_1 e_{\omega_{N_1}}$$

$$\ddot{v}_{N_1} = \ddot{v}_{N_1}^{\text{ref}} - (k_1+k_2)\dot{e}_{v_{N_1}} - (k_1 k_2 + \gamma_2) e_{v_{N_1}}$$

reusing the gains of (16), (18) where $\dot{\omega}_{N_1}, \ddot{v}_{N_1}$ are computed by using $\dot{u}_{\text{user}}$ which is provided by the device and smooth enough during the simulations. We also introduce some haptic feedback to assist the user: 1) preventing a crash to the ground; 2) leveling the flight path; and 3) ensuring sufficient forward velocities. Note that other types of control (e.g., mission planner) can be applied to the leader UAV.

The simulations are performed with 25-trailing fixed-wing UAVs. We set the relative position vector (expressed in $\{\mathcal{N}_{j+1}\}$) to be $l_j = (3, 0, 0)^T[\text{m}]$ for $j = 1, 2, \cdots 24$ to render the line-topology platoon, although other formation shapes are possible with suitably-chosen $l_j \in \mathbb{R}^3$ with $l_j^{(1)} > 0$. The virtual frame gains are chosen as $b_\omega = 3, k_\omega = 1, b_\vartheta = 1, k_\vartheta = 1, k_h = 0.5, \gamma_1 = 0.1, k_1 = 10, \gamma_2 = 1, k_2 = 1$ and the local control gains as $b_a = 4, k_a = 4, \epsilon = 1, \gamma = 16, k = 48, k_r = 1, k_s = 1$. Conditions for the gain selection are provided in Section II and Section III, with their values needed to be tuned for specific systems under those conditions. Parameters of the fixed-wing UAVs are determined according to [19], e.g., the mass $m_j = 1.72[\text{kg}]$ and aerodynamic coefficients $C_Z^0 = 0.1601, C_Z^\alpha = 4.4851, C_Y^\beta = 0.7076, C_X^0 = 0.01\,602, C_X^A = 0.1347$. The aerodynamic force is written by

$$f_j^v(\rho, v_j) = -0.5\rho A_j \|v_j\|_2^2 \begin{pmatrix} C_j^X & C_j^Y & C_j^Z \end{pmatrix}^T$$

where $A_j = 0.285[\text{m}^2]$ is the wing area, $\rho = 1.22[\text{kg/m}^3]$ is the air density, $v_j \in \mathbb{R}^3$ is the relative wind velocity. The aerodynamic coefficients $C_j^\star$ are given by $C_j^Z := C_Z^0 + C_Z^\alpha \sin\alpha_j, C_j^Y := C_Y^\beta \sin\beta_j, C_j^X := C_X^0 + C_X^A (C_j^Z)^2$ where $\alpha_j = \sin^{-1}(e_3^T v_j/\|v_j\|)$ is the angle of attack and $\beta_j = \sin^{-1}(e_2^T v_j/\|v_j\|)$ is the side-slip angle. Aerodynamic uncertainties are modeled by estimated aerodynamic coefficients $\bar{C}_Z^0 = 0.15, \bar{C}_Z^\alpha = 4.5, \bar{C}_Y^\beta = 0.7, \bar{C}_X^0 = 0.015, \bar{C}_X^A = 0.15$ and included in the simulations. The body acceleration is assumed to be measurable (e.g., accelerometer).

The real-time simulation environment (i.e., visual display, physics simulation, haptic interface, etc.) is custom built using

[1]https://www.forcedimension.com/

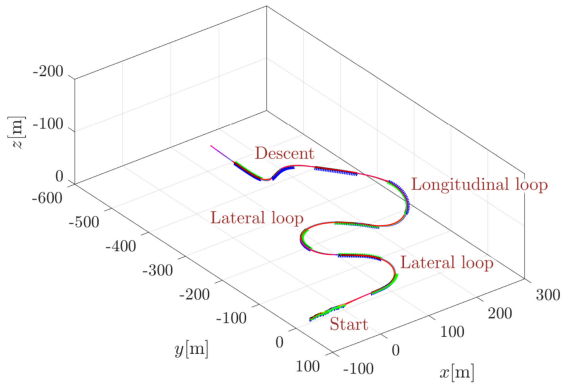

(a) Flight path of 25 fixed-wing UAVs. Black lines indicate the formation of the UAVs for every 10[s].

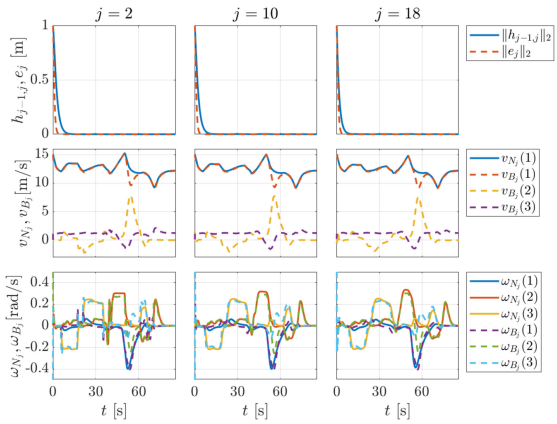

(b) Formation objective $h_{j-1,j}$ and tracking objective e_j of the three agents, $j = 2, 10, 18$. Twist of VNFs and UAVs are also provided.

Fig. 4. Real-time simulation results of the teleoperated platooning with 25 fixed-wing UAVs and $\mathbb{E}(3)$ haptic device, showing the efficacy of the virtual frame and local control layers (i.e., $h_{j,j+1} \to 0$ and $e_j \to 0$) with boundedness of all relevant states and the regulated sideways velocity (link to multimedia (video): https://youtu.be/Z3Mo66KIsns).

C++ and OpenGL. The dynamics of the physical fixed-wing UAVs and the virtual evolution of the VNFs are integrated with the explicit Euler method. Simulation results and link to multimedia (video) are presented in Fig. 4. Initial formation errors $h_{j,j+1}(t = 0)$ and initial tracking errors $e_j(t = 0)$ are chosen to be random with magnitude $1[\mathrm{m}]$. Initial velocities of the VNFs and the UAVs are $15[\mathrm{m/s}]$, and the initial attitudes are identical. The user command for the simulation in Fig. 4 is lateral loop around $t = 5$–$16, 21$–$35[\mathrm{s}]$, longitudinal loop around $t = 40$–$50[\mathrm{s}]$, and descent around $t = 60$–$70[\mathrm{s}]$. The formation objective (i.e., $h_{j,j+1}$) and the tracking objective (i.e., e_j) converge to zero, implying that the UAVs attain the desired platoon formation. The side velocity $v_{B_j}^{(2)}$ is also regulated due to the heading control, and converges to zero at level flight. Adequate angle of attack (or downward velocity $v_{B_j}^{(3)}$) is formed to generate the lift force during the simulation.

V. Conclusion

We proposed a novel distributed control framework for a teleoperated platooning of 3D fixed-wing UAVs consists of: 1) virtual frame layer, which renders a platooning of 3D virtual nonholonomic frames (VNFs) with only peer-to-peer communication required; and 2) local control layer, which drives each fixed-wing UAV to track corresponding VNF with the underactuated property and aerodynamic uncertainty considered. Real-time human-in-the-loop simulations are also performed to show the theory. Some possible future research directions include: 1) incorporation of collision avoidance and formation feedback [20]; 2) extension to other communication topologies both for cooperative perception or control; and 3) experimentation with real fixed-wing UAVs.

References

[1] D. J. Lee, "Passive decomposition and control of nonholonomic mechanical systems," *IEEE Trans. Robot.*, vol. 26, no. 6, pp. 978–992, Dec. 2010.
[2] "Mercedes benz automates runway snow clearance with truck platooning," Oct. 2017, [Online]. Available: https://www.theengineer.co.uk/mercedes-benz-truck-platooning/.
[3] C. Ha, Z. Zuo, F. B. Choi, and D. J. Lee, "Passivity-based adaptive backstepping control of quadrotor-type UAVs," *Robot. Auton. Syst.*, vol. 62, no. 9, pp. 1305–1315, 2014.
[4] R. C. Nelson *et al.*, *Flight Stability and Automatic Control*., vol. 2 New York: WCB/McGraw Hill, 1998.
[5] D. M. Stipanović, G. Inalhan, R. Teo, and C. J. Tomlin, "Decentralized overlapping control of a formation of unmanned aerial vehicles," *Automatica*, vol. 40, no. 8, pp. 1285–1296, 2004.
[6] H. G. De Marina, Z. Sun, M. Bronz, and G. Hattenberger, "Circular formation control of fixed-wing UAVs with constant speeds," in *Proc. IEEE/RSJ Int. Conf. Intell. Robots Syst.*, 2017, pp. 5298–5303.
[7] K. Fathian, T. H. Summers, and N. R. Gans, "Distributed formation control and navigation of fixed-wing UAVs at constant altitude," in *Proc. Int. Conf. Unmanned Aircr. Syst.*, 2018, pp. 300–307.
[8] F. Xie, X. Zhang, R. Fierro, and M. Motter, "Autopilot-based nonlinear UAV formation controller with extremum-seeking," in *Proc. IEEE Conf. Decis. Control*, 2005, pp. 4933–4938.
[9] R. W. Beard, T. W. McLain, D. B. Nelson, D. Kingston, and D. Johanson, "Decentralized cooperative aerial surveillance using fixed-wing miniature UAVs," *Proc. IEEE Proc. IRE*, vol. 94, no. 7, pp. 1306–1324, Jul. 2006.
[10] M. Bergou, M. Wardetzky, S. Robinson, B. Audoly, and E. Grinspun, "Discrete elastic rods," *ACM Trans. Graph.*, vol. 27, no. 3, 2008, pp. 63:1–63:12.
[11] C. Heintz and J. B. Hoagg, "Formation control for agents modeled with extended unicycle dynamics that includes orientation kinematics on $\mathsf{SO}(m)$ and speed constraints," *Syst. Control Lett.*, vol. 146, 2020, Art. no. 104784.
[12] C. Heintz and J. B. Hoagg, "Formation control for fixed-wing UAVs modeled with extended unicycle dynamics that include attitude kinematics on $\mathsf{SO}(m)$ and speed constraints," in *Proc. Amer. Control Conf.*, 2020, pp. 883–888.
[13] R. Sepulchre, M. Jankovic, and P. V. Kokotovic, *Constructive Nonlinear Control*. London: Springer-Verlag, 1997.
[14] D. J. Lee, "Distributed backstepping control of multiple thrust-propelled vehicles on a balanced graph," *Automatica*, vol. 48, no. 11, pp. 2971–2977, 2012.
[15] C. Ha, J. Yoon, C. Kim, Y. Lee, S. Kwon, and D. J. Lee, "Teleoperation of a platoon of distributed wheeled mobile robots with predictive display," *Auton. Robots*, vol. 42, no. 8, pp. 1819–1836, 2018.
[16] M. Waszak, J. Davidson, and P. Ifju, "Simulation and flight control of an aeroelastic fixed wing micro aerial vehicle," in *Proc. AIAA Atmospheric Flight Mechanics Conf. Exhibit*, 2002, Art. no. 4875.
[17] W. Khan and M. Nahon, "Modeling dynamics of agile fixed-wing UAVs for real-time applications," in *Proc. Int. Conf. Unmanned Aircr. Syst.*, 2016, pp. 1303–1312.
[18] A. Cho, J. Kim, S. Lee, and C. Kee, "Wind estimation and airspeed calibration using a UAV with a single-antenna gps receiver and pitot tube," *IEEE Trans. Aerosp. Electron. Syst.*, vol. 47, no. 1, pp. 109–117, Jan. 2011.
[19] J. Shen, Y. Su, Q. Liang, and X. Zhu, "Calculation and identification of the aerodynamic parameters for small-scaled fixed-wing UAVs," *Sensors*, vol. 18, no. 1, 2018, Art. no. 206.
[20] P. Ogren, M. Egerstedt, and X. Hu, "A control lyapunov function approach to multi-agent coordination," in *Proc. IEEE Conf. Decis. Control*, vol. 2. 2001, pp. 1150–1155.